2023

# Poly(1,2-glycerol carbonate) nanoparticles for delivery of hydrophilic therapeutic

BOSTON UNIVERSITY

COLLEGE OF ENGINEERING

Thesis

# POLY(1,2-GLYCEROL CARBONATE) NANOPARTICLES FOR DELIVERY OF HYDROPHILIC THERAPEUTICS

by

**YUYANG GU**

B.S., Shenyang Pharmaceutical University, 2019

Submitted in partial fulfillment of the

requirements for the degree of

Master of Science

2023

Approved by

First Reader

Mark W. Grinstaff, Ph.D.
William Fairfield Warren Distinguished Professor
Distinguished Professor of Translational Research
Professor of Biomedical Engineering
Professor of Chemistry
Professor of Materials Science and Engineering
Professor of Medicine

Second Reader

Wilson W. Wong, Ph.D.
Associate Professor of Biomedical Engineering

Third Reader

Arturo Vegas, Ph.D.
Assistant Professor of Chemistry
Assistant Professor of Biomedical Engineering
Assistant Professor of Materials Science and Engineering

ACKNOWLEDGEMENTS

I would like to thank my advisor Prof. Mark Grinstaff for having me in his lab. It is in this wonderful lab that I have had the opportunity to grow as a well-rounded person. He himself has always been a role model to me and inspired me to think more and work harder. I really appreciate his support and advice. I would also like to thank Prof. Wilson Wong and Prof. Arturo Vegas for their help and advice on my project.

I would like to thank my mentor Dr. Ting-Yu Shih. He guided me on research and trained me to have good practices and habits which are beneficial not only for my research but also for my future development in general. I truly appreciate his support and help in so many aspects of life.

I would like to thank my lab mates for creating a fantastic working environment. Thank you to Brett Tingley for a lot of helpful discussions and advice. Thank you to Alina Ringaci, Jenny Korunes-Miller, Matt Taylor, Dr. Robbie Sabatelle, Dr. Eric Bressler, Dr. Jack Kirsch, Josh McGee for teaching me lab techniques and helping me troubleshoot.

Last but not least, I would like to thank my family for their generous support.

**POLY(1,2-GLYCEROL CARBONATE) NANOPARTICLES FOR DELIVERY OF HYDROPHILIC THERAPEUTICS**

**YUYANG GU**

ABSTRACT

Hydrophilic therapeutics, including a wide range of peptides, proteins and small molecule drugs, play a pivotal role in biomedicine. To overcome their unfavorable pharmacokinetics such as rapid clearance and poor permeability through lipid membranes, various delivery strategies based on liposomes, solid lipid nanoparticles, lipophilic prodrugs have been investigated. However, the toxicity associated with the systemic administration of these formulations limits their applications. Previously, we developed poly(1,2-glycerol carbonate) nanoparticles (PGC NPs) that readily entrap a hydrophobic small molecule drug and deliver it to peritoneal tumors post intraperitoneal injection. Here, we designed PGC NPs capable of loading hydrophilic drugs with high efficiency. The Cy5-BSA loaded NPs achieved a high encapsulation efficiency of 92.97% and drug loading of 3.55 wt%, with sustained release for one week. AntiPD1-loaded NPs reached ~100% encapsulation efficiency and released a substantial dose of antibodies by day 7. The secondary structure of polyclonal antibodies loaded in the NPs was not affected by the formulation process, as demonstrated by the characteristic peaks and valleys on the CD spectra. Minimal cytotoxicity to NIH/3T3 and MSTO-211H/Luc cells was observed after treatment with up to 1.5 mg/mL blank NPs over 24 hours, indicating biosafety of the NPs. Additionally, a promising assay was developed for assessing anti-PD1/PDL1 efficacy *in vitro*. Our findings suggest that PGC NPs loaded with hydrophilic drugs hold potential as

safe and effective drug delivery systems.

TABLE OF CONTENTS

LIST OF FIGURES

LIST OF ABBREVIATIONS

| | |
|---|---|
| API | Active pharmaceutical agents |
| BCS | Bovine calf serum |
| BGE | Rac-benzyl glycidyl ether |
| BSA | Bovine serum albumin |
| CAR | Chimeric Antigen Receptor |
| CD | Circular dichroism spectroscopy |
| Cy5 | Cyanine5 |
| Cy5-BSA | Cy5-labeled bovine serum albumin |
| DCM | Dichloromethane |
| DI | Deionized |
| DL | Drug loading by weight |
| DLS | Dynamic light scattering |
| DMSO | Dimethyl sulfoxide |
| EDC | N-(3-Dimethylaminopropyl)-N'-ethylcarbodiimide hydrochloride |
| EE | Encapsulation efficiency |
| ELISA | Enzyme-linked immunosorbent assay |
| FBS | Fetal bovine serum |
| IC | Immune checkpoints |
| ICIs | Immune checkpoint inhibitors |
| IFN-γ | Interferon gammaTNF |
| IgG | Immunoglobulin G |
| MDSCs | Myeloid-derived suppressor cells |

| | |
|---|---|
| MWCO | Molecular weight cutoff |
| NHS | N-Hydroxysuccinimide |
| NPs | Nanoparticles |
| pAb | Polyclonal antibody |
| PBS | Phosphate-buffered saline |
| PC | L-α-phosphocholine |
| PCL-PGC-C18 | Poly(glycerol monostearate co-Ɛ-caprolactone) polymer |
| PD1 | Programmed cell death protein1 |
| PDL1 | Programmed death ligand-1 |
| PGC | Poly(1,2-glycerol carbonate) |
| PLGA | Poly(lactic-co-glycolic acid) |
| PVA | Poly(vinyl alcohol) |
| Rho-BSA | Rhodamine-labeled bovine serum albumin |
| siRNA | Small interfering RNA |
| TCR | T-cell receptor |
| TME | Tumor microenvironment |
| TNF-α | Tumor necrosis factor alpha |
| Tregs | Regulatory T cells |

# CHAPTER 1: INTRODUCTION AND BACKGROUND

## 1.1. Nanoparticle-based drug delivery systems provide numerous advantages

Nanoparticles are particles with sizes at the nanoscale level. They possess unique and beneficial chemical and biological properties, which make them suitable for a wide range of biomedical applications such as drug delivery, imaging, and tissue engineering[1].

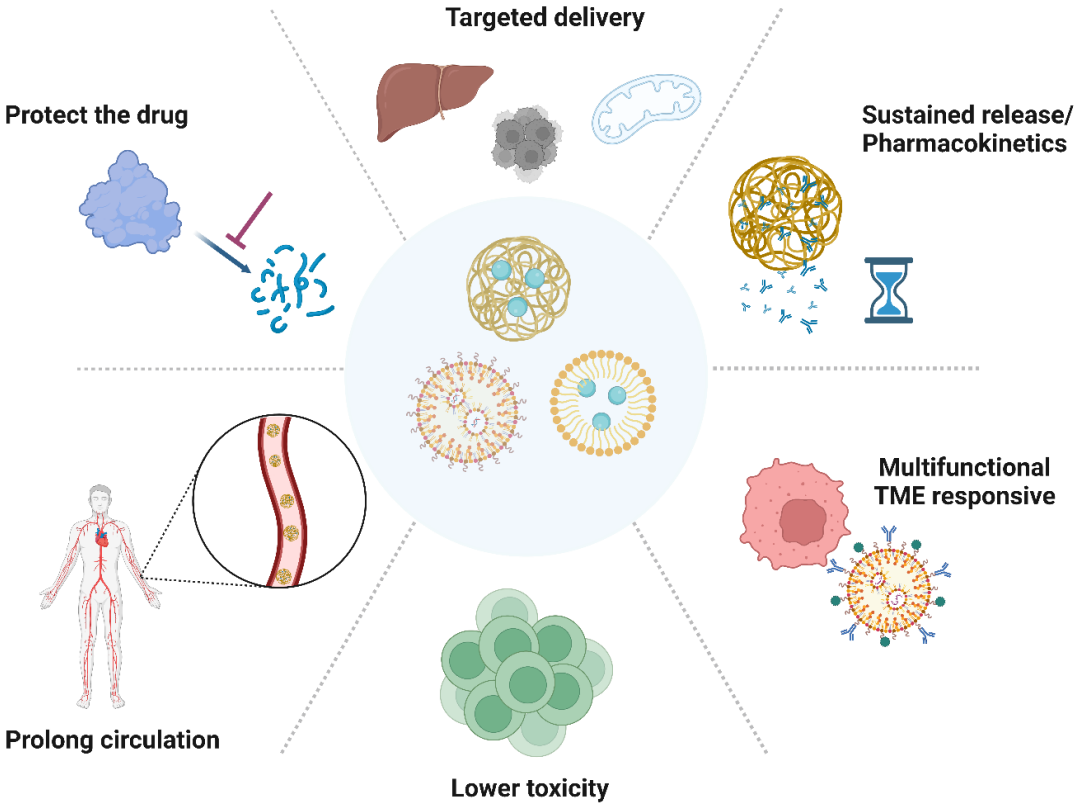


**Figure 1-1.** Advantages of nanoparticles. Created with BioRender.com.

Nanoparticle-based drug delivery systems provide multiple advantages (**Figure 1-1**). For example, (1) by loading drugs into NPs, the degradation rate of drugs by enzyme in the human body can be decreased; (2) rationally designed NPs can achieve targeted delivery to tumor tissue, specific organs or organelles such as the liver[2-4], and mitochondria[5-7]; (3) NPs can provide sustained drug release or other specified pharmacokinetic profiles[8-10]; (4)

some NPs can be multifunctional and responsive to the tumor microenvironment (TME)[11,12]; (5) NPs can lower toxicity and prolong the circulation of drugs[13,14].

## 1.2. Glycerol polymers have demonstrated great potential for drug delivery

Glycerol polymers are macromolecules synthesized from glycerol or its derivatives. They have been widely investigated for use as drug delivery platforms, ophthalmic sealants, antibacterial agents and coatings for seromas[15].

Al Subeh *et al.* utilized the polymer poly(glycerol monostearate co-Ɛ-caprolactone) (PCL-PGC-C18) to create Eupenifeldin-loaded meshes, which prevented cancer recurrence when used after lung cancer surgery in an animal study[16]. Another polymer poly(1,2-glycerol carbonate) was used to produce double-loaded NPs that both chemically conjugated and physically entrapped the drug paclitaxel. This delivery system achieved ultra-high drug loading, improved the solubility of the otherwise poorly water-soluble drug and achieved tumor localization. Most importantly, *in vivo* studies demonstrated that it improved the overall survival compared to conventional paclitaxel formulations[17,18].

## 1.3. Poly(1,2-glycerol carbonate) is a biocompatible and biodegradable polymer

Poly(1,2-glycerol carbonate) is a member of the glycerol polymer family and possesses a lot of advantages. First, it can be deprotected to remove the benzyl group on the side chain, yielding a free hydroxyl group that can be further functionalized[18,19]. Second, it is both biodegradable and biocompatible, making it an ideal choice for biomedical applications. Third, PGC is a versatile polymer that can be fabricated into nanoparticles and meshes. Fourth, PGC is amorphous in nature, but through compositional

modifications, semicrystalline materials can be produced for a wide range of applications[15,20].

### 1.4. Hydrophilic drugs make up a significant portion of biomedicine

The active pharmaceutical ingredients (API) can be classified as hydrophilic or hydrophobic drugs based on their solubility in water or lipid-containing solution[21]. More specifically, hydrophilic drugs with solubility > 1000 mg/mL are considered highly soluble, those with solubility of 33–100 mg/mL are considered soluble and those with solubility of 10–33 mg/mL are sparingly soluble[22].

In the space of hydrophilic therapeutics, there exist different types of proteins such as insulin, cytokines like interferon-gamma, and monoclonal antibodies. Many small molecule drugs are also hydrophilic, such as the chemotherapeutic doxorubicin, antibiotics ciprofloxacin and antiviral drug cidofovir[23]. Additionally, genetic medicine such as siRNA, mRNA and plasmid DNA also exhibit high hydrophilicity[14].

However, the hydrophilic nature of these therapeutics can lead to many undesirable physiological properties, e.g., low permeability through physiological barriers, short circulation time, non-ideal biodistribution, and low bioavailability[14,24].

### 1.5. Poly(1,2-glycerol carbonate) nanoparticles are promising delivery platforms for hydrophilic therapeutics

Previously, we developed PGC NPs that achieved ultra-high drug loading of the hydrophobic drug paclitaxel, realized tumor localization, and improved the therapeutic outcomes in animal studies[17-19]. However, no hydrophilic drugs have been loaded into the PGC NPs. In this study, we aim to develop a delivery platform for hydrophilic drugs using

poly(1,2-glycerol carbonate) as the carrier. Specifically, our first goal is to investigate how various process parameters affect the characteristics of the NPs, such as size, drug loading, encapsulation efficiency and release kinetics. The second objective is to develop an assay for assessing the *in vitro* efficacy of protein therapeutic anti-PD1/PDL1 antibodies, which we intend to load into the PGC NPs as a model drug.

# CHAPTER 2: NANOPARTICLE SYNTHESIS AND CHARACTERIZATION

## 2.1. INTRODUCTION

Double emulsions have been employed for encapsulating both hydrophilic and hydrophobic drugs, and they offer several advantages over single emulsions, particularly for hydrophilic drug delivery. In oil-in-water single emulsions, hydrophilic drugs tend to diffuse and partition into the continuous aqueous phase, leading to low encapsulation efficiency, while double emulsions can overcome this issue. Additionally, double emulsions can achieve better control over the drug release[25,26].

Water-in-oil-in-water emulsion is the one of the most common types of double emulsion for hydrophilic drug encapsulation. A two-step procedure is usually adopted for synthesis where the inner aqueous phase and oil phase are mixed and sonicated to form the primary emulsion, which is then dispersed in the outer aqueous phase to form the double emulsion[27].

Numerous promising drug delivery systems have been developed using the double emulsion technique. For example, Chiang *et al.* prepared a pH-sensitive Trastuzumab-conjugated nanocapsules loaded with both hydrophilic doxorubicin and hydrophobic paclitaxel that achieved targeted delivery and enhanced anti-tumor efficacy[28]. Park *et al.* developed dexamethasone-loaded poly(lactic-co-glycolic acid) (PLGA) NPs which were coated with siRNA for the treatment of rheumatoid arthritis[29].

Here, we examined the influence of various process parameters involved in the double emulsion-solvent evaporation method on the characteristics of NPs. The parameters tested are sonication time, surfactant type and concentration, phase volume ratios, the amount of

input proteins. A library of NPs with a diverse range of characteristics were synthesized and characterized.

## 2.2. MATERIALS AND METHODS

### 2.2.1 Materials

Bis(triphenylphosphoranylidene)ammonium chloride (PPNCl), rac-benzyl glycidyl ether (BGE), rhodamine B, N-(3-Dimethylaminopropyl)-N'-ethylcarbodiimide hydrochloride (EDC), N-Hydroxysuccinimide (NHS), L-α-phosphocholine (PC), poly(vinyl alcohol) (M.W.:13,000-23,000) (PVA), sodium hydroxide, sodium bicarbonate, Span™ 80 were purchased from Sigma-Aldrich. Dichloromethane (DCM), methanol, dimethyl sulfoxide (DMSO) were obtained from Greenfield Global. Bovine serum albumin (BSA) was acquired from Goldbio. Cyanine5 N-Hydroxysuccinimide ester (Cy5-NHS) was purchased from Lumiprobe. Sonics Vibra-Cell VCX-600 Ultrasonic Processor was bought from Sonics & Materials, Newtown, CT. Human IgG affinity purified was obtained from Innovative Research. Phosphate-buffered saline (PBS) was obtained from Gibco. Dialysis membrane (MWCO: 300,000) was purchased from Spectrum. Pierce BCA protein assay kit, dialysis tubing (MWCO: 10,000) were purchased from Thermo Scientific. Centrifugal units (Molecular weight cut off, MWCO: 100,000 or 300,000) were bought from Merck Millipore Ltd. and Sartorius, UK. Brookhaven 90Plus Particle Size Analyzer was obtained from Brookhaven Instruments Corporation, Holtsville, NY. Syringe filter (PVDF, 0.22μm) was acquired from Advangene. The CellTiter 96® Aqueous One Solution Cell Proliferation Assay was purchased from Promega, Madison, WI.

2.2.2 Synthesis of poly (1,2-glycerol carbonate)

Poly (1,2-glycerol carbonate) was synthesized by the alternating copolymerization of epoxide and $CO_2$, as previously described[18]. Briefly, in a glovebox, 10 mg of SalcyCo$^{III}$Cl and 10 mg of PPNCl were added to the reactor. Then 1.52 mL of BGE was added dropwise. The mixture was reacted with $CO_2$ at 400 psi at 40℃ overnight. The crude product was dissolved in DCM and then precipitated dropwise in excess cold methanol in conical tubes twice. The conical tubes were centrifuged at 1500 ×g for 5 min to collect the purified polymer. The polymer was stored at -20℃ until use.

2.2.3 Synthesis of Rhodamine-BSA

Rhodamine-labeled bovine serum albumin (Rho-BSA) was synthesized by EDC coupling. Rhodamine b, EDC, NHS and BSA were mixed and stirred for 17 hours at room temperature. The product was dialyzed against deionized (DI) water for 24 hours to remove free dye. Rho-BSA was lyophilized and stored at -20℃ until use.

2.2.4 Synthesis of Cy5-BSA

0.771 mg of Cy5-NHS was dissolved in 0.4 mL of DMSO. 20 mg of BSA was dissolved in 3.6 mL of 0.1 M bicarbonate at pH 8.5. Cy5-NHS ester was then added to BSA. The reaction was allowed to run at 4℃ overnight. The Cy5-labeled bovine serum albumin (Cy5-BSA) was dialyzed against nanopure water for 24 hours to remove free dye. Cy5-BSA was stored at 4℃ until use.

2.2.5 Nanoparticles synthesis

Protein-loaded PGC NPs were synthesized using a double emulsion-solvent evaporation method[30,31]. BSA, Rho-BSA, Cy5-BSA, polyclonal antibodies, anti-PD1

antibodies were used as model drugs. The typical fabrication procedure is described below unless specified otherwise. Briefly, the proteins were dissolved in PBS to form the inner aqueous phase. PGC and PC were dissolved in DCM to form the organic phase. The inner aqueous phase and organic phase were mixed and sonicated to form the primary emulsion. The primary emulsion was then added to PVA solution and sonicated to form the double emulsion. The double emulsion was then transferred to a 0.25% PVA solution and stirred for 3 hours at room temperature to evaporate DCM.

### 2.2.6 Nanoparticles collection and purification

The NPs were collected and purified by one of the following three ways. (1) Centrifugal units. The NP suspension was centrifuged at 3220 g for 30 min each round and then washed twice with nanopure water; (2) Ultracentrifugation. The speed and duration tested were 15,000 g for 15 min, 25,000 g for 25 min. The NP suspension was collected and washed twice with nanopure water; (3) Dialysis. The NPs were dialyzed against nanopure water for 24 hours.

### 2.2.7 Nanoparticles diameter and PDI

The hydrodynamic diameter and PDI of the NPs were measured by dynamic light scattering (DLS). 50 μL of NPs were diluted in 3 mL of nanopure water for DLS measurement.

### 2.2.8 Encapsulated proteins extraction

Encapsulated Proteins were measured by two different extraction methods. (1) 20 mg of lyophilized NPs were dissolved in 0.25 mL of DCM, followed by the addition of 0.5 mL of nanopure water. The mixture was vortexed for 5 min and then centrifuged at 3,000 rpm

for 5 minutes. This vortexing and centrifugation procedure was repeated four times. The BSA concentration in the upper aqueous phase was measured using either Nanodrop or BCA assay. (2) 20 mg of lyophilized NPs were dissolved in 2 mL of 1M sodium hydroxide for 30 min. The fluorescence of the fluorescently labelled protein was then detected.

### 2.2.9 Encapsulation efficiency and drug loading measurement

The percent drug loading by weight (DL) and encapsulation efficiency (EE) were determined by measuring the fluorescence intensity of Rho-BSA/Cy5-BSA. DL was calculated as the mass of encapsulated proteins divided by the mass of the NPs. EE was calculated as the mass of encapsulated proteins divided by the mass of proteins initially added.

### 2.2.10 Nanoparticle release study

To study the release kinetics, a suspension containing 7 mL of Cy5-BSA-loaded NPs was placed into dialysis tubing and incubated at 37℃ with continuous shaking in 150 mL of PBS. At predetermined time points, 700 μL of release medium was withdrawn and the protein concentration was measured by fluorescence intensity. 700 μL of fresh PBS was added to replenish the release medium.

### 2.2.11 Protein secondary structure via circular dichroism (CD) spectroscopy

Blank NPs and polyclonal antibody (pAb)-loaded NPs were synthesized and collected using centrifugal filter units. The released pAbs were collected via dialysis. The release medium of blank NPs was used as the baseline for CD measurement.

### 2.2.12 Nanoparticle Cytotoxicity

Lyophilized blank NPs were resuspended in cell culture media at a concentration of 3

mg/mL. The resuspended NPs were filtered using a 0.22 μm sterile syringe filter. NIH/3T3 and MSTO-211H/luc cells were seeded at a density of 5,000 cells/well in a 96-well plate and allowed to adhere overnight. The cells were then treated with serial dilutions of the NP suspension for 24 hours. After treatment, the media was removed, and cell viability was assessed using the CellTiter 96® Aqueous One Solution Cell Proliferation Assay. Cell viability was calculated as the absorbance of the NP-treated groups divided by that of the untreated group.

## 2.3 RESULTS

### 2.3.1 Effect of sonication time on blank NP characteristics

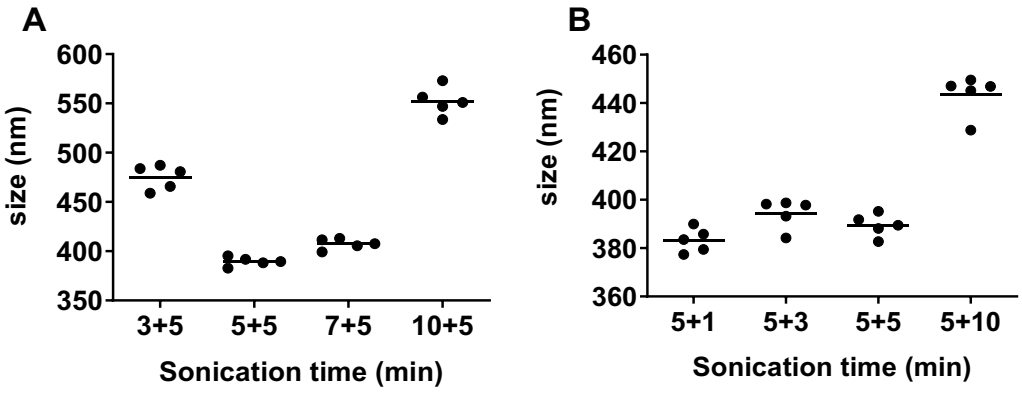


**Figure 2-1.** Effect of sonication time on blank NP characteristics. (A) Size of blank NPs with different second sonication time to make the double emulsion. (B) Size of blank NPs with different first sonication time to make the primary emulsion.

Blank NPs were synthesized with varying sonication times. The effect of the first sonication time on NP size was test with the second sonication time set to 5 min. When the first sonication time was increased from 3 min to 7 min in step of 2 min, the NP size decreased initially and then plateaued. When the time was further increased to 10 min, the

NP size increased (**Figure 2-1-A**). This result suggests that over-sonication could potentially destroy the double emulsion. On the other hand, no significant difference in NP size was observed when increasing the second sonication time from 1 to 5 min. When further increasing the time to 10 min, the NP size increased (**Figure 2-1-B**).

2.3.2 Effect of surfactant concentration in outer aqueous phase on blank NP characteristics

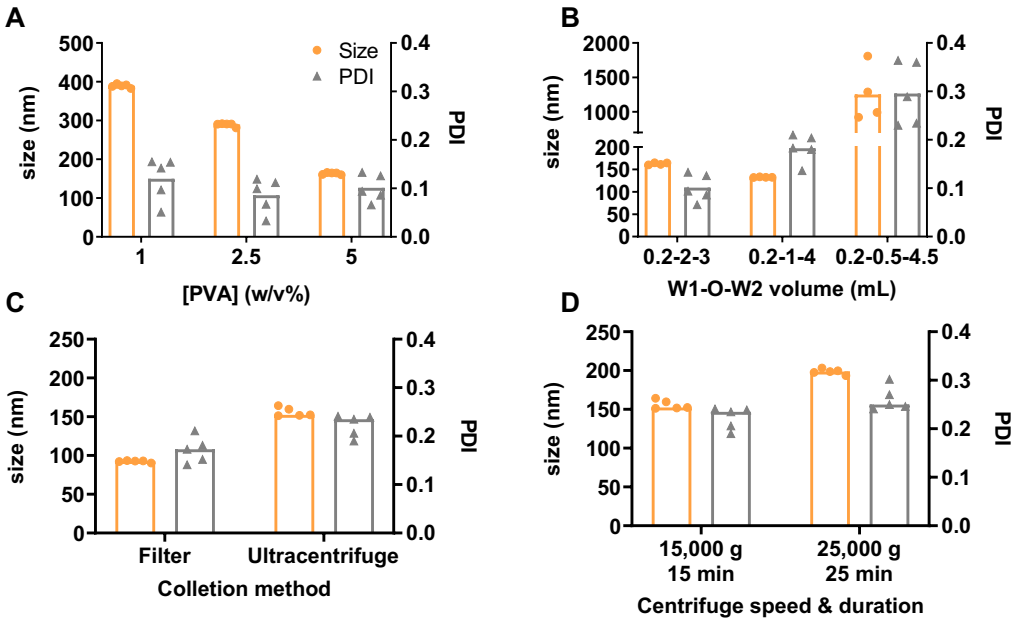


**Figure 2-2.** Effect of PVA concentration, phase volume ratios, collection method on NP characteristics. Size and PDI of blank NPs (A) made with different concentrations of PVA in the outer aqueous phase; (B) made with different phase volume ratios; (C) collected by centrifugal filter units or ultracentrifugation; (D) collected by ultracentrifugation at different speeds and durations.

Blank NPs were synthesized with different PVA concentration in the outer aqueous phase. When the PVA concentration was increased from 1% to 5%, NP size decreased with

minor fluctuations in PDI (**Figure 2-2-A**).

2.3.3 Effect of phase volume ratio on blank NP characteristics

Blank NPs were synthesized with 5% PVA in the outer aqueous phase and 5-min sonication for both primary and double emulsion formation. When the phase volume ratio of the inner aqueous phase to oil phase to outer aqueous phase was changed from 0.2:2:3 to 0.2:1:4, NP size decreased with a slight increase in PDI. When the phase volume ratio was 0.2:0.5:4.5, NP size increased to the micrometer scale with a PDI around 0.3 (**Figure 2-2-B**).

2.3.4 Effect of collection method on blank NP characteristics

Blank NPs were synthesized with 5% PVA in the outer aqueous phase, phase volume ratio of 0.2:1:4, and 5-min sonication for both primary and double emulsion formation. The NPs were then collected by either centrifugal filter units or ultracentrifugation. Ultracentrifugation speeds and durations of 15,000 g for 15 min and 25,000 g for 25 min were tested. Smaller nanoparticles with narrower size distribution were obtained using filter units (**Figure 2-2-C)**. Increasing the ultracentrifugation speed and duration resulted in an increase in NP size, while the PDI remained at a similar level (**Figure 2-2-D**).

2.3.5 Effect of surfactant type in the primary emulsion on blank NP characteristics

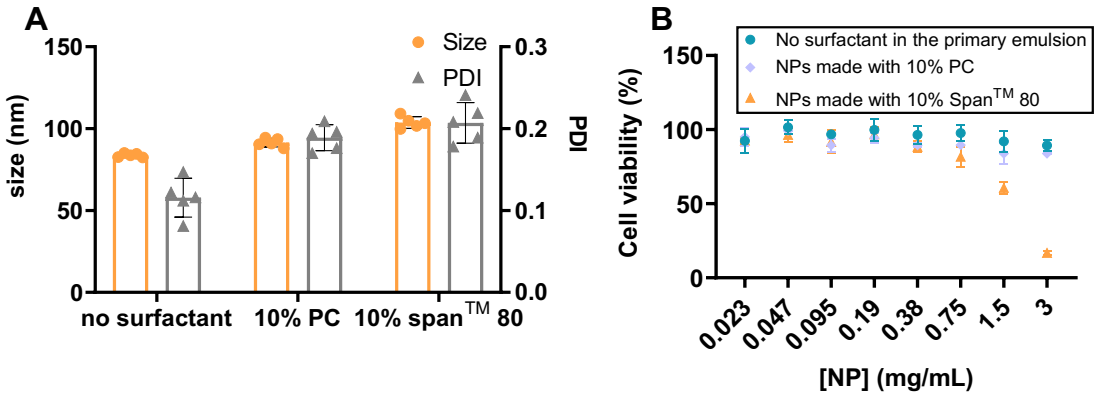


**Figure 2-3.** Effect of surfactant type in the primary emulsion on blank NP characteristics. (A) Size and PDI; (B) cytotoxicity profile of blank NPs made with different surfactants in the primary emulsion.

Blank NPs were synthesized with different surfactants in the primary emulsion. The addition of surfactant in the primary emulsion resulted in an increase in NP size and PDI compared to NPs synthesized without surfactant in the primary emulsion. The Span™ 80 group had a slightly larger size (~105 nm) and PDI than the phosphatidylcholine (PC) group (~92 nm) (**Figure 2-3-A**).

Minimal cytotoxicity to NIH/3T3 cells was observed after treatment with up to 3 mg/mL of blank NPs made with or without 10% PC in the primary emulsion for 24 hours. However, a significant decrease in cell viability was observed for blank NPs made with 10% Span™ 80 in the primary emulsion at NP concentration of 0.75 mg/mL and above (**Figure 2-3-B**), indicating that span™ 80 is more cytotoxic than PC.

2.3.6 Effect of surfactant concentration in the primary emulsion on Rho-BSA loaded NP characteristics

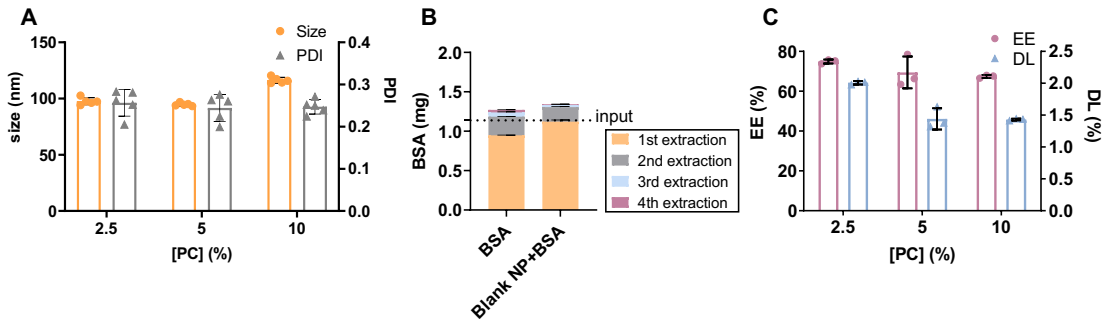


**Figure 2-4.** Effect of surfactant concentration in the primary emulsion on Rho-BSA loaded NP characteristics. (A) Size and PDI of Rho-BSA loaded NPs made with different PC concentrations in the primary emulsion. (B) Validation of the extraction method used to measure the amount of encapsulated proteins in NPs. (C) Encapsulation efficiency and drug loading by weight of NPs made with different PC concentration in the primary emulsion.

Rho-BSA loaded NPs were synthesized with different PC concentrations in the primary emulsion. Increasing PC concentration from 2.5% to 5% to 10% did not significantly affect the NP size and PDI (**Figure 2-4-A**).

Encapsulation efficiency (EE) was defined as the mass of encapsulated proteins divided by the mass of proteins initially added. Drug loading (DL) was defined as the mass of encapsulated proteins divided by the mass of nanoparticles. The mass of encapsulated proteins was determined using either a direct extraction method or back calculation by measuring the mass of unencapsulated proteins. To validate the extraction method, we used experimental groups of BSA only or BSA with blank NPs and carried out the extraction procedure. It was shown that two rounds of extraction were sufficient to detect nearly all

the proteins initially added. For the BSA with blank NPs group, the amount of BSA recovered was slightly higher than the input amount, indicating that the NP formulation slightly interferes with the extraction and measurement (**Figure 2-4-B**).

When decreasing the PC concentration from 10% to 5% to 2.5%, EE slightly increased but overall maintained at a similar level. However, DL increased significantly from ~1.5% to ~2% (**Figure 2-4-C**).

2.3.7 Effect of the amount of input proteins on Rho-BSA loaded NP characteristics

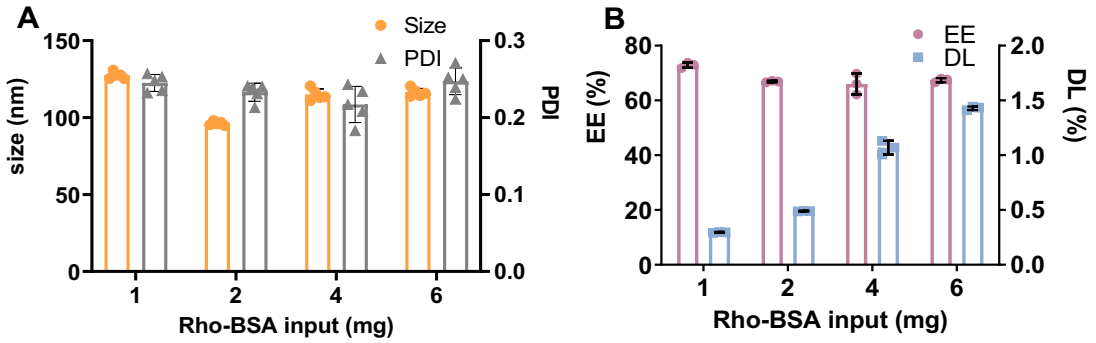


**Figure 2-5.** Characteristics of Rho-BSA loaded PGC NPs. (A) Size and PDI; (B) Encapsulation efficiency and drug loading by weight of Rho-BSA loaded NPs with input of 1, 2, 4, 6 mg of Rho-BSA.

When input amount of Rho-BSA was increased from 1 mg to 6 mg, the NP size remained below 130 nm, with the 2 mg group having a size below 100 nm. The PDI of all groups was at a similar level of ~0.25 (**Figure 2-5-A**).

With 10% PC in the primary emulsion, increasing the input amount of Rho-BSA from 1 mg to 6 mg increased the DL while maintaining the EE at approximately 70% (**Figure 2-5-B**), suggesting that the loading capacity of the NPs has not yet been reached.

2.3.8 Blank PGC NPs exhibited minimal cytotoxicity to MSTO-211H/Luc and NIH/3T3 cells

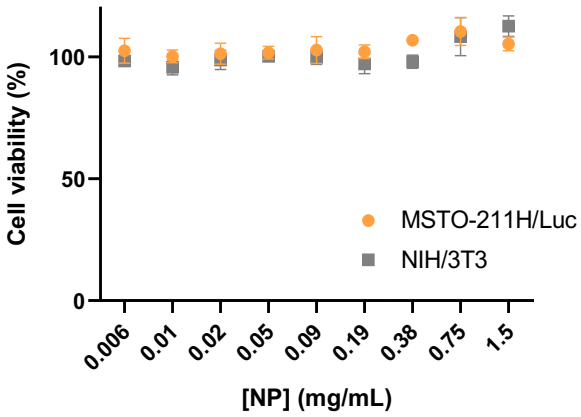


**Figure 2-6.** Cytotoxicity profile of blank PGC NPs to MSTO-211H/Luc and NIH/3T3 cells.

Minimal cytotoxicity to MSTO-211H/Luc and NIH/3T3 cells was observed after treatment with up to 1.5 mg/mL blank PGC NPs for 24 hours **(Figure 2-6)**, indicating the excellent biosafety of the blank PGC NPs.

2.3.9 Cy5-BSA loaded PGC NP release kinetics

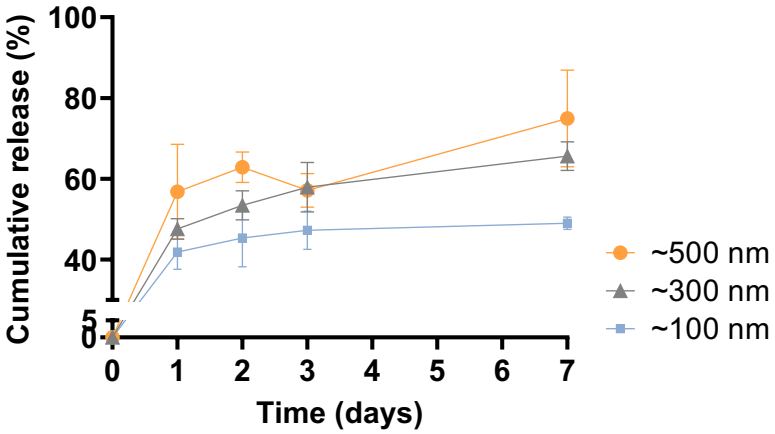


**Figure 2-7.** Cy5-BSA release kinetics from PGC NPs at 37 ℃ in pH 7.4 PBS.

Cy5-BSA loaded NPs with different sizes were prepared by varying the sonication time, resulting in NPs with average sizes of ~100, ~300, and ~500 nm for sonication times of 1+1 min, 3+3 min, and 5+5 min, respectively. The larger NPs exhibited faster protein release (**Figure 2-7**).

On the first day, there was ~40-60% burst release, followed by a slower release rate of ~2-6% on day 2 and 3. From day 4 onwards, the release rate further decreased and maintained a slow release until day 7.

2.3.10 Protein secondary structure retained after formulation

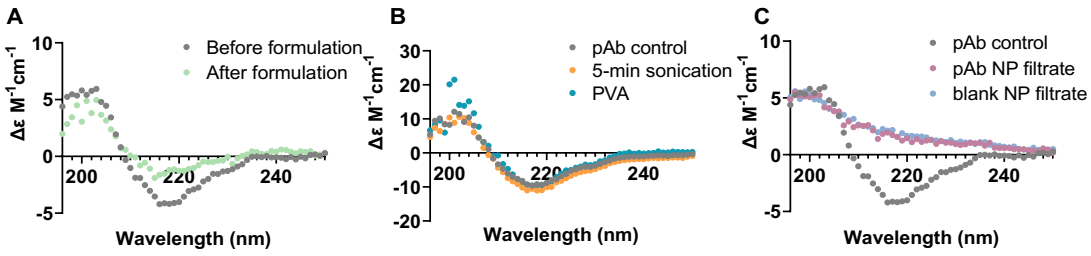


**Figure 2-8.** Circular dichroism (CD) spectra of polyclonal antibodies under different conditions. (A) CD spectra of pAbs before formulation and after being released from NPs. (B) CD spectra of pAbs without disturbance, after 5-min sonication and mixed with 10% PVA. (C) CD spectra of pAbs before formulation and in the filtrate which was below the detection limit.

The secondary structure of polyclonal antibody was retained after the NP formulation process, as evidenced by the characteristic peaks (~200 nm) and valleys (~220 nm) observed in the CD spectra (**Figure 2-8-A**). After the perturbation with some of the key procedures involved in the NP formulation process, such as through sonication or mixing with 10% PVA, the CD spectra of the pAbs remained approximately the same as that

without perturbation (**Figure 2-8-B**), further confirming the minimal impact of the formulation process on the protein structure. When the concentration of pAbs was too low, e.g. the amount in the filtrate when collecting NPs by centrifugal filter units, no characteristic valley (~220 nm) was observed and the entire curve was above the x-axis (**Figure 2-8-C**). The CD spectra of the pAbs after direct perturbance in panel B showed better similarity with the natural pAbs than that in the release medium. This may be due to the interference of other chiral compounds in the release medium.

2.3.11 Anti-PD1 antibody loaded NP characteristics

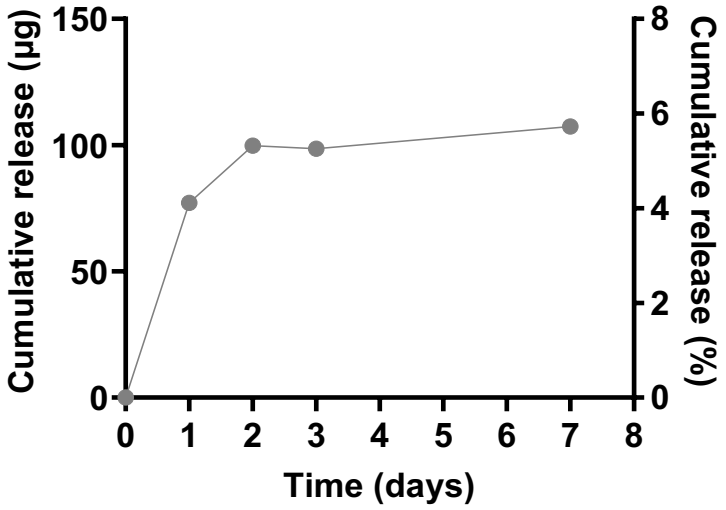


**Figure 2-9.** Anti-PD1 antibody release kinetics from PGC NPs at 37 ℃ in pH 7.4 PBS.

The anti-PD1 (aPD1) loaded NPs showed a much slower drug release than BSA loaded NPs. There was ~4% release on day 1, followed by ~1% on day 2 **(Figure 2-9)**. The release rate further decreased from day 3 onwards. By day 7, there was a total of ~6% release.

## 2.4 DISCUSSIONS

In this study, the process parameters were adjusted to synthesize nanoparticles with a wide range of sizes, spanning from approximately 90 nm to 600 nm. Nanoparticle size has a significant impact on its properties and *in vivo* pharmacokinetics. Specifically, the NP size measured immediately after formulation can affect its actual size in a physiological setting due to differences in aggregation, degradation, disassembly, stiffness, and corona formation[32]. In addition, NP size directly affect cellular interactions and pharmacokinetic profiles, such as biodistribution, circulation time and cellular uptake[33,34]. Thus, this library of NPs with various sizes can be utilized for different scenarios based on specific design requirements.

The Cy5-BSA loaded NPs showed an encapsulation efficiency of 92.97% and drug loading by weight of 3.55 wt%, while the anti-PD1 loaded NPs showed nearly 100% encapsulation efficiency. These values are comparable to or better than those reported in the literature for NPs synthesized using the double emulsion-solvent evaporation method, which typically have an encapsulation efficiency of less than 80% [25,35-39]. However, the amount of encapsulated proteins was calculated as the difference between the initially added proteins and the unencapsulated proteins present in the dialysis media or filtrate. There might be overestimation of the actual loading since protein loss could occur during the formulation process, and incomplete dialysis may result in underestimation of the unencapsulated proteins.

Anti-PD1 antibodies showed a much slower release rate compared to BSA in the first week. This may have to do with the difference in molecular weight (Mw) or size of these

two proteins. Since the Mw of anti-PD1 antibody (~150 kDa) is much larger than that of BSA (~66 kDa), it is more difficult for the antibodies to diffuse through the pores on the NPs. It is also known that PGC has a slow degradation rate which is on the order of weeks, meaning that the protein release due to polymer degradation mechanisms is minimal in the first week. The two mechanisms altogether explain the slower release of anti-PD1[40]. Even though only ~6% antibodies were released by day 7 with the absolute protein release being ~100 μg, this dose is comparable to those typically used in murine studies[41-43]. On the other hand, the release kinetics can be affected by the release media. It may be necessary to use a release medium that better mimics the physiological conditions of the administration route for *in vivo* study. Additionally, it was reported that the polymer poly(trimethylene carbonate) (PTMC) can be degraded by lipases[44,45], there may be enzymes present in the human body that can degrade PGC. Therefore, we may design a delivery system that is responsive to these endogenous or exogenous enzymes to realize better control over the release behavior.

The release rate of Cy5-BSA loaded NPs was found to be dependent on the size of the NPs, with larger NPs exhibiting faster release in the first week. This can be attributed to the diffusion-based release mechanism, where larger NPs have larger pore sizes that allow for faster diffusion of the proteins out of the polymer matrix.

As for whether the antibodies released from NPs retain their bioactivity and antigen binding affinity, the amount of released proteins was determined by sandwich ELISA where the PD1 protein was used to capture the analyte anti-PD1 antibodies. This assay served as a preliminary test of the binding affinity. Alternatively, fluorescently labelled

anti-PD1 can be loaded into the NPs. Then the affinity of the released antibodies to PD1 on living T cells can be determined by measuring the fluorescence via flow cytometry.

Another important characteristic of NPs is their stability in body fluids such as serum. In our study, we plan to use intraperitoneal injection, which means that a limited amount of NPs will enter the bloodstream and the NPs will mainly take effect in the tumor tissues. Therefore, it is important to test the stability of the NPs in extracellular fluids or other solutions that could mimic the tumor microenvironment.

In summary, we synthesized a library of NPs with different characteristics in terms of size, drug loading and release kinetics by adjusting the process parameters. We also confirmed that the formulation process had a negligible effect on the secondary structure of the antibodies loaded into the NPs. Moreover, the blank PGC NPs showed excellent biosafety profiles. These findings demonstrate the great potential of PGC NPs as an effective drug delivery platform for hydrophilic therapeutics.

# CHAPTER 3: ASSAY DEVELOPMENT FOR ASSESSING THE EFFICACY OF ANTI-PD1/PDL1 ANTIBODIES *IN VITRO*

## 3.1. INTRODUCTION

### 3.1.1. Challenges of CAR T cell therapy against solid tumors

Chimeric Antigen Receptor (CAR) T cell therapy is a type of cancer treatment for which T cells are genetically modified to express synthetic receptors that can target specific antigens on the tumor surface. It has shown great success in blood cancer treatment, with six CAR T cell therapies approved by FDA as of Nov 2022, among which four CARs are CD19-directed and two are BCMA-directed[46].

However, the performance of CAR T cell therapy in solid tumors has been limited due to multiple challenges such as (1) poor trafficking and insufficient infiltration of CAR T cells to tumors; (2) inhibitory soluble factors and cytokines present in the tumor microenvironment; (3) suppressive immune cells like regulatory T cells (Tregs) and myeloid-derived suppressor cells (MDSCs); (4) upregulation of inhibitory receptors on T cells like programmed cell death protein 1 (PD1)[46].

### 3.1.2. PD1/PDL1 pathway and delivery of anti-PD1/PDL1 antibodies

Programmed cell death protein 1/programmed cell death 1 ligand 1 (PD1/PDL1) pathway is one of the most well-known immune checkpoints (ICs). PD1 is expressed on the surface of activated T cells. Its ligands PDL1 is commonly upregulated on tumor cells likely due to IFN-γ[47,48]. Upon binding of PD1 to PDL1, the immune responses mediated by T cells are impaired through multiple mechanisms, such as T cell apoptosis, exhaustion,

anergy, induction of IL-10 and differentiation of Tregs[47]. It was also reported that this inhibitory pathway hindered T-cell receptor (TCR) signaling and CD28 co-stimulation[49]. The immune checkpoint inhibitors (ICIs) have become a standard of care for a range of cancer types, with seven anti-PD1/PDL1 mAbs approved by FDA as of Nov 2022[50].

The systemic delivery of anti-PD1/PDL1 resulted in low response rate and severe toxicity. In contrast, nanoplatforms such as liposomes, lipid nanoparticles, polymeric nanoparticles and inorganic nanoparticles demonstrated great promises in improving anti-PD1/PDL1 efficacy and safety by promoting tumor infiltrations, prolonging blood circulation and realizing spatial-temporal control of drug release[51-53].

### 3.1.3. Combinatorial therapy of CAR T cells with anti-PD1/PDL1 antibodies

It was reported that the low objective response rates to ICIs might be due to the lack of preexisting anti-tumor immune responses[54]. T cells that exist around the tumors while exhausted might be essential for ICIs to take effects. For this reason, CAR T cell therapy that can trigger robust antitumor immune response together with ICIs, can potentially achieve excellent synergistic tumor killing efficacy.

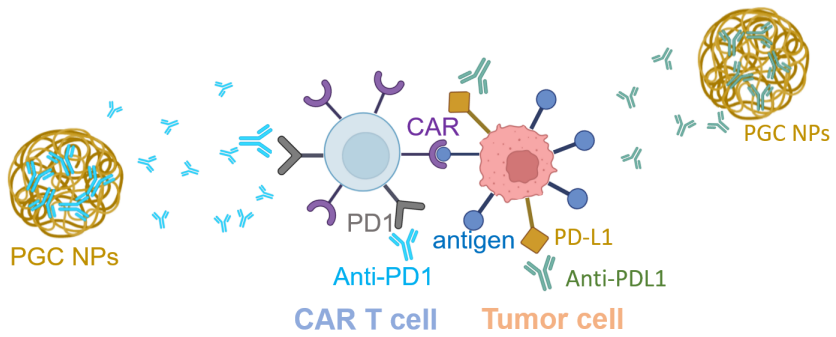


**Figure 3-1.** Immunomodulation of tumor microenvironment by targeted delivery and sustain release of anti-PD1/PDL1 antibodies from PGC NPs. Created with BioRender.com.

In order to evaluate the efficacy of anti-PD1/PDL1 antibodies in enhancing the tumor-killing capabilities of CAR T cells, we proposed to pre-treat tumor cells with cytokines to upregulate the PDL1 level on their surface so that the effect of the PD1/PDL1 pathway blockade can be amplified and easier to detect. We optimized the following conditions for this assay: (1) type and concentration of cytokines; (2) ratio of CAR T cells to tumor cells; (3) concentration of anti-PD1/PDL1.

## 3.2. MATERIALS AND METHODS

### 3.2.1. Materials

Dulbecco's Modified Eagle Medium, RPMI 1640 medium were purchased from Corning. Bovine calf serum (BCS) was bought from Sigma-Aldrich. Fetal bovine serum (FBS) was acquired from R&D Systems, Inc. Penicillin−streptomycin, 0.25% Trypsin-EDTA and T cell expansion basal medium were obtained from Gibco. Flow cytometer was produced by attune. Bright-Glo™ Luciferase Assay was purchased from Promega, Madison, WI. CD279 (PD-1) mouse anti-Human-APC and rabbit anti-Human IgG (H+L) secondary antibody were acquired from thermos fisher scientific. InVivoSIM anti-human PD-1 (Pembrolizumab Biosimilar) and InVivoSIM anti-human PDL1 (Atezolizumab Biosimilar) were purchased from BioXcell.

### 3.2.2. Cell culture

MSTO-211H cells and MSTO-211H transfected with the firefly luciferase gene (MSTO-211H/Luc) were cultured in RPMI 1640 media supplemented with 10% FBS and 1% penicillin−streptomycin. NIH/3T3 cells were cultured in DMEM media supplemented with 10% BCS and 1% penicillin−streptomycin. CAR T cells and un-transduced T cells

were cultured in Optimizer media. All cells were maintained at 37°C with 5% $CO_2$ in a humidified incubator.

3.2.3. Cytotoxicity of IFN-γ and TNF-α

MSTO-211H/Luc cells were seeded in a 96-well white opaque plate at 5,000 cells/well and were allowed to adhere overnight. The cells were then treated with IFN-γ or TNF-α for 24 or 48 hours. The cell viability was determined with the Bright-Glo™ Luciferase Assay.

3.2.4. PDL1 expression level on MSTO-211H/Luc cells after treatment with cytokines

MSTO-211H/Luc cells were seeded in a 24-well flat-bottom tissue culture plate at 30,000 cells/well and were allowed to adhere overnight. The cells were then treated with serial dilutions of IFN-γ or TNF-α. After 24 or 48 hours, media was removed. Cells were detached using Versene solution and then transferred to a 96-well U-bottom TC plate. The cells were then stained with anti-PDL1-APC antibodies or an isotype control at room temperature for 40 minutes. The cells were then washed twice with FACS buffer. The fluorescence intensity and percentage of PDL1 positive MSTO-211H/Luc cells were measured by flow cytometry.

3.2.5. PD-1 expression level on activated CAR T cells

MSTO-211H/Luc cells were seeded in a 48-well flat-bottom tissue culture plate at 15,000 cells/well and were allowed to adhere overnight. CAR T cells were added to MSTO-211H/Luc cells at E:T ratios of 16:1, 8:1, 4:1, 2:1, 1:1. After 24 hours, the supernatant was transferred to a 96-well U-bottom plate. T cells were collected and stained with anti-PD1-APC or an isotype control at room temperature for 40 minutes. Then the T cells were washed twice with FACS buffer. The fluorescence intensity and percentage of PD1 CAR T

cells were measured by flow cytometry.

3.2.6. Anti-PD1 and anti-PDL1 antibody dose screening

MSTO-211H/Luc cells were seeded in a 96-well white opaque plate at 5,000 cells/well and were allowed to adhere overnight. A serial dilution of anti-PD1 or anti-PDL1 antibodies were added to the MSTO-211H/Luc cells. Then CAR-T cells were added at an E:T ratio of 2:1. After 24 hours, the cell viability was determined using the Bright-Glo™ Luciferase Assay.

3.2.7. Anti-tumor efficacy of CAR-T cells with/without immune checkpoint inhibitors in the presence/absence of cytokines

MSTO-211H/Luc cells were seeded in a 96-well white opaque plate at 5,000 cells/well and were allowed to adhere overnight. For the cytokine-treated groups, cells were treated with IFN-γ or TNF-α at specific concentrations. After 24 hours, CAR-T cells that were cultured in media containing ICIs were added at E:T ratios of 16:1, 8:1, 4:1, 2:1. After 24 hours, the cell viability was determined using the Bright-Glo™ Luciferase Assay.

3.2.8. Statistical analysis

Non-paired student's t tests were conducted to assess the significant differences between groups. Statistical significance was reported by * for $p \leq 0.05$. ** for $p \leq 0.01$. *** for $p \leq 0.001$.

## 3.3. RESULTS

### 3.3.1. Cytotoxicity of IFN-γ and TNF-α

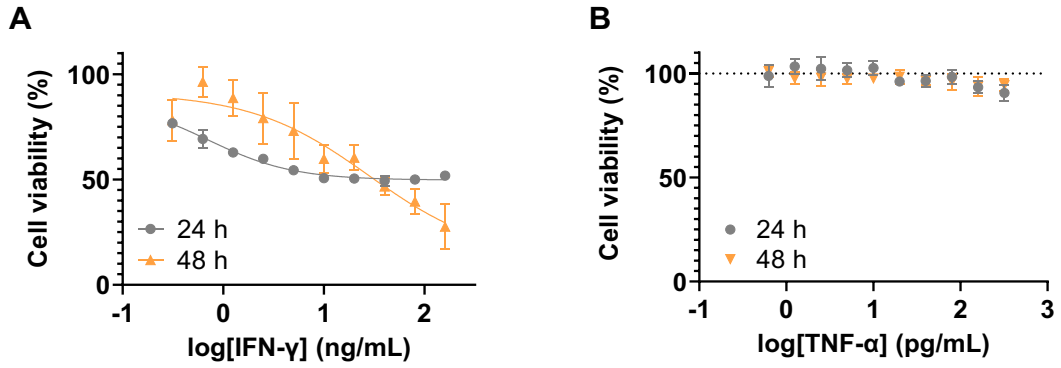


**Figure 3-2.** Cell viability of MSTO-211H/Luc cells after treatment with (A) IFN-γ or (B) TNF-α for 24 h and 48 h.

The MSTO-211H/Luc cells were treated with a serial dilution of IFN-γ from 160 ng/mL to 0.3125 ng/mL. IFN-γ is cytotoxic to MSTO-211H/Luc in a dose dependent manner (**Figure 3-2-A**). After 24-hour treatment, the cell viability decreased as the IFN-γ concentration increased. When the concentration of IFN-γ was greater than or equal to 10 ng/mL, the cell viability was maintained at ~50%. After 48-hour treatment, the cell viability exhibited a descending trend from ~100% to 27.6% as the IFN-γ concentration increased. The $IC_{50}$ value obtained from the 48-hour dose response curve was 28.05 ng/mL.

The MSTO-211H/Luc cells were treated with a serial dilution of TNF-α from 320 pg/mL to 0.625 pg/mL. After 24-hour and 48-hour treatment, the cell viability remained above 95% except for the highest dose (**Figure 3-2-B**). TNF-α showed minimal cytotoxicity to the MSTO-211H/Luc cell line at 320 pg/mL with a cell viability of ~90%.

3.3.2. Effect of IFN-γ and TNF-α on PDL1 level on MSTO-211H/Luc cells

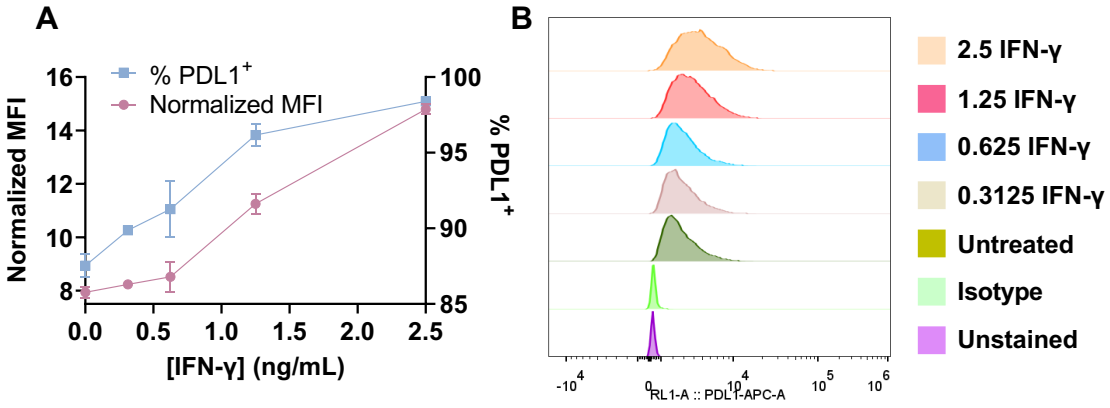


**Figure 3-3.** PDL1 level on MSTO-211H/Luc cells after treatment with IFN-γ for 24 hours. (A) Normalized MFI and percentage of PDL1 positive cells for; (B) Representative histograms of PDL1 for MSTO-211H/Luc treated with different concentrations of IFN-γ.

The MSTO-211H/Luc cells were treated with different concentrations of IFN-γ. The PDL1 level was then measured by flow cytometry. The percentage of PDL1$^+$ MSTO-211H/Luc cells increased from ~87.5% for the wild type to ~98% for the highest-dose IFN-γ treated group. when the IFN-γ concentration increased from 0.3125 ng/mL to 0.625 ng/mL, the normalized MFI slightly increased compared to the wild type. When further increasing the IFN-γ concentration to 2.5 ng/mL, the normalized MFI increased to 14.79 (**Figure 3-3-A**).

The histogram for the untreated group compared to the isotype and unstained showed that there was a basal expression of PDL1 on MSTO-211H/Luc cells. IFN-γ upregulated the PDL1 level on MSTO-211H cells in a dose-dependent manner (**Figure 3-3-B**). When increasing the IFN-γ concentration, the PDL1 level increased.

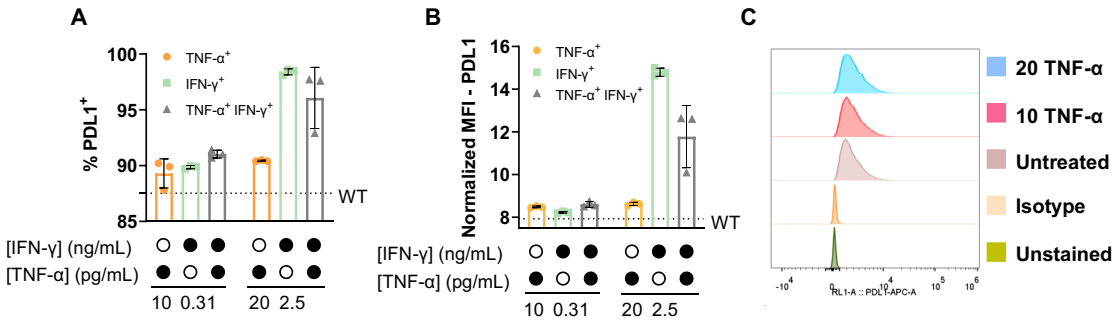


**Figure 3-4.** PDL1 level on MSTO-211H/Luc cells after treatment with TNF-α and/or IFN-γ for 24 hours. (A) Percentage of PDL1 positive cells for; (B) Normalized MFI of PDL1 for; (C) Representative histograms of PDL1 for MSTO-211H/Luc treated with different concentrations of TNF-α and/or IFN-γ.

The percentage of PDL1$^{+}$ MSTO-211H/Luc cells and Normalized MFI of PDL1 for the IFN-γ$^{+}$ TNF-α$^{+}$ group followed similar trends as the IFN-γ$^{+}$ TNF-α$^{-}$ group, indicating IFN-γ played a dominant role in upregulating PDL1 level at the concentrations tested (**Figure 3-4-A, B**). The representative histograms confirmed that TNF-α barely upregulated the PDL1 level at concentration as high as 20 pg/mL (**Figure 3-4-C**).

3.3.3. PD1 expression level on CAR T cells upon activation at different E:T ratios

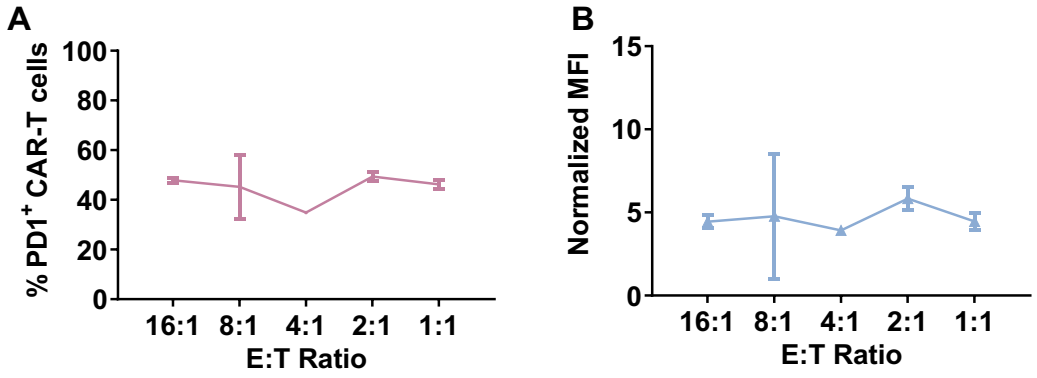


**Figure 3-5.** PD1 level on CAR-T cells upon activation by MSTO-211H/Luc cells without cytokines pre-treatment.

The percentage of PD1$^+$ CAR-T cells and normalized MFI maintained at similar levels across different E:T ratios (**Figure 3-5**). Since the number of CAR-T cells was always greater than the number of tumor cells for every E:T ratio, only a small subset of CAR-T cells was able to contact the tumor cells, be activated and then express PD1.

3.3.4. Anti-PD1 and anti-PDL1 doses screening

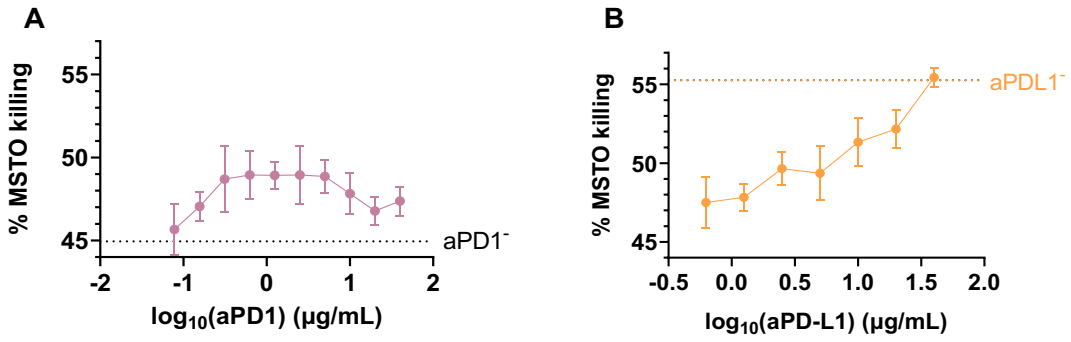


**Figure 3-6.** Percentage of MSTO-211H/Luc killed by CAR-T cells at E:T ratio of 2:1 in the presence of (A) anti-PD1 or (B) anti-PDL1 antibodies at different concentrations.

As shown in section 3.3.3, the PD1 level on activated CAR T cells were similar across

different E:T ratios, therefore, one of the ratios, 2:1 was used for the anti-PD1 dose screening. The tumor killing efficacy improved as the concentration of anti-PD1 antibody increased from 78 ng/mL to 312.5 ng/mL, followed by a flatten region when the concentration of anti-PD1 antibody increased from 312.5 ng/mL to 5 μg/mL. The tumor killing efficacy then started to decrease when the anti-PD1 concentration was greater than 5 μg/mL (**Figure 3-6-A**). But overall the tumor killing were with a similar range. Based on previous cytotoxicity data, anti-PD1 concentration of greater than 5 μg/mL showed obvious toxicity to MSTO-211H/Luc cells. It is speculated that at such concentration, it is cytotoxic to CAR-T cells as well.

In the presence of anti-PDL1, the tumor killing efficacy showed an ascending trend as the concentration of anti-PDL1 increased from 312 ng/mL to 40 μg/mL (**Figure 3-6-B**). Overall, the dynamic range was minimal (~10%). The reason for weaker tumor killing in the aPDL1$^{+}$ groups than in the aPDL1$^{-}$ group, except at the highest concentration where the tumor killing efficacy were similar, might be due to contamination as the wells of the aPDL1$^{-}$ group were right next to the highest dose group, and the operator didn't change pipette tips when adding CAR-T cells.

3.3.5. No significant anti-tumor efficacy improvement of CAR T cells was observed with anti-PD1/PDL1 antibodies without cytokines pre-treatment

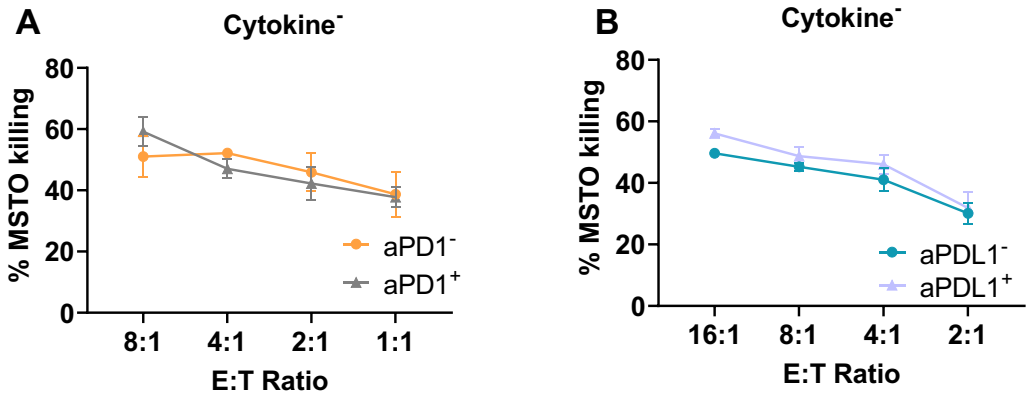


**Figure 3-7.** MSTO-211H/Luc killing by CAR-T cells at different E:T ratios with and without (A) anti-PD1; (B) anti-PDL1 antibodies in the absence of cytokines.

MSTO-211H/Luc cells and CAR-T cells were cocultured at different ratios for 24 hours. No significant anti-tumor efficacy improvement of CAR T cells was observed with 20 μg/mL anti-PD1/PDL1 antibodies (**Figure 3-7-A,B)**.

3.3.6. No significant anti-tumor efficacy improvement of CAR T cells was observed with anti-PD1 antibodies when pre-treating MSTO-211H/Luc with IFN-γ

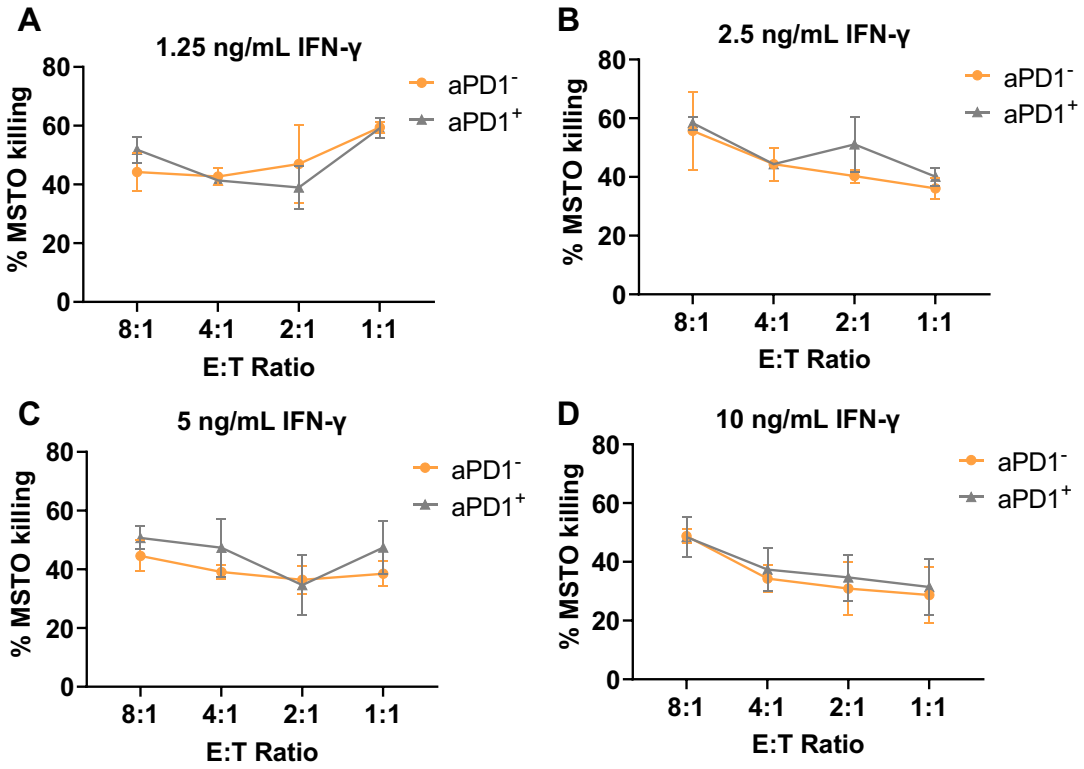


**Figure 3-8.** MSTO-211H/Luc killing by CAR-T cells at different E:T ratios with and without anti-PD1 antibodies when the MSTO-211H/Luc cells were pre-treated with (A) 1.25 ng/mL; (B) 2.5 ng/mL; (C) 5 ng/mL; (D) 10 ng/mL IFN-γ for 24 hours.

After treating MSTO-211H/Luc cells with different concentrations of IFN-γ, CAR-T cells were then added to and cocultured with tumor cells at different ratios in the presence or absence of anti-PD1 antibodies for 24 hours. No significant anti-tumor efficacy improvement of CAR T cells was observed with 20 μg/mL anti-PD1 antibodies. For the 1.25 ng/mL IFN-γ pre-treated group, the aPD1$^-$ curve didn't follow a descending trend as the E:T ratio decreased (**Figure 3-8-A, B, C, D**).

3.3.7. No significant anti-tumor efficacy improvement of CAR T cells was observed with anti-PDL1 antibodies when pre-treating MSTO-211H/Luc with IFN-γ

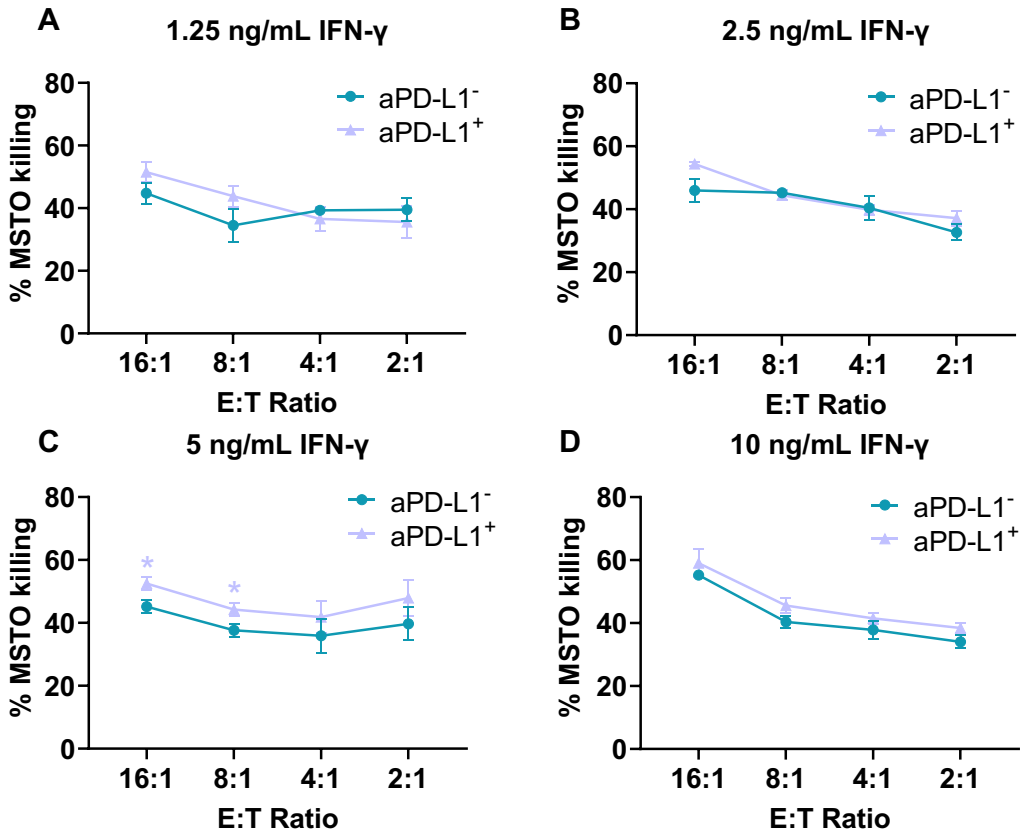


**Figure 3-9.** MSTO-211H/Luc killing by CAR-T cells at different E:T ratios with and without anti-PDL1 antibodies when the MSTO-211H/Luc cells were pre-treated with (A) 1.25 ng/mL; (B) 2.5 ng/mL; (C) 5 ng/mL; (D) 10 ng/mL IFN-γ for 24 hours.

After treating MSTO-211H/Luc cells with different concentrations of IFN-γ, CAR-T cells were then added to and cocultured with tumor cells at different ratios in the presence or absence of anti-PDL1 antibodies for 24 hours. No significant anti-tumor efficacy improvement was observed with 20 μg/mL anti-PDL1 antibodies for most of the experimental groups. However, when pre-treating MSTO-211H/Luc cells with 5 ng/mL

IFN-γ for 24 hours, a significant improvement on tumor killing efficacy of CAR-T cells was observed at E:T ratios of 16:1 and 8:1 (**Figure 3-9-A, B, C, D**).

3.3.8. Significant anti-tumor efficacy improvement of CAR T cells was observed with aPD1/PDL1 when pre-treating MSTO-211H/Luc with TNF-α

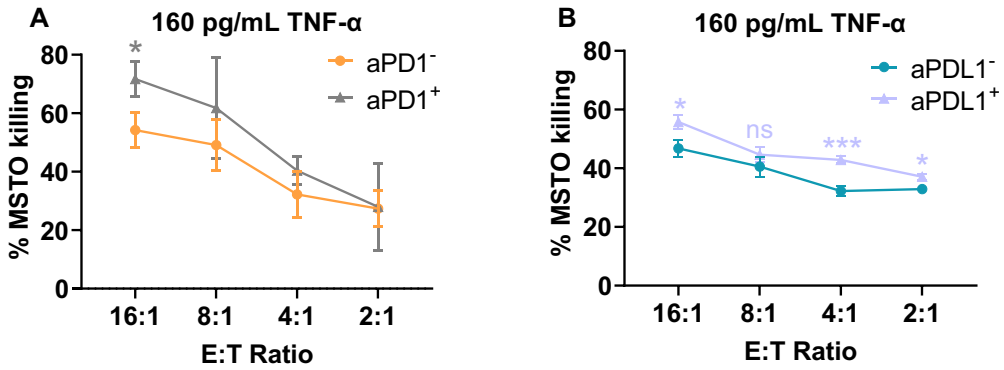


**Figure 3-10.** MSTO-211H/Luc killing by CAR-T cells at different E:T ratios with and without (A) anti-PD1; (B) anti-PDL1 antibodies when the MSTO-211H/Luc cells were pre-treated with 160 pg/mL TNF-α for 24 hours.

When pre-treating MSTO-211H/luc cells with 160 pg/mL TNF-α for 24 hours, there was a significant enhancement on tumor-killing efficacy of CAR-T cells at E:T ratios of 16:1 with anti-PD1 antibodies (**Figure 3-10-A**). In the presence of anti-PDL1 antibodies, significant anti-tumor efficacy improvement was observed at E:T ratios of 16:1, 4:1 and 2:1. Among these groups, 4:1 group showed the highest degree of improvement (**Figure 3-10-B**).

## 3.4. DISCUSSIONS

The assay developed using MSTO-211H/Luc cells demonstrated a significant improvement in anti-tumor efficacy of CAR T cells in the presence of anti-PD1/PDL1 antibodies, which is comparable to what has been reported in literature using the same cell line[55]. However, the dynamic range was limited. As the cytotoxicity of IFN-γ to MSTO-211H/Luc cells was high, this cell line appeared to be vulnerable and sensitive. For mesothelioma cells, it may be more appropriate to use other cell lines such as MPP89, IST-MES1 and IST-MES2 as these have shown successful upregulation of PDL1 levels with IFN-γ treatment[56]. However, before testing the PDL1 upregulation level, it is important to investigate the cytotoxicity of IFN-γ to these proposed cell lines. Previous studies did show that IFN-γ could activate pronecrotic and prosurvival signaling pathways, and initiate tumor cell apoptosis in general[57,58]. Another approach could be to introduce the gene that encodes PDL1 to the tumor cells by transfection or transduction.

Alternatively, breast cancer cell lines such as MCF-7, MDA-MB-231, HCC38[59,60], which have a higher basal level of PDL1, could be used to avoid the use of cytokines. Cytokines can exert more physiological effects other than upregulating PDL1 level on tumor cells, which may hinder the anti-tumor efficacy of CAR-T cells through pathways or mechanisms that are not fully understood or investigated yet. This makes the assay less predictable. Therefore, using tumor cell lines with higher basal PDL1 levels may be a better approach to investigate the anti-tumor efficacy improvement of CAR-T cells in the presence of anti-PD1/PDL1 antibodies.

It is possible that the PDL1 level on tumor cells and PD1 level on CAR T cells are

adequate. There are other conditions to be considered to improve the assay. These include: (1) the time course to conduct the killing assay; (2) the quality and binding affinity of the anti-PD1/PDL1 antibodies in nature; (3) other endpoint measurement besides the percentage of tumor killing, such as CAR T cell activation levels; (4) using a three-dimensional cell culture model that better mimics the *in vivo* environment.

In summary, we developed a promising *in vitro* assay to assess the efficacy of anti-PD1/PDL1 antibodies. A significant improvement in the tumor-killing capabilities of CAR T cells was observed in the presence of anti-PD1/PDL1 antibodies when the mesothelioma cell line MSTO-211H/Luc was pre-treated with TNF-α.

# BIBLIOGRAPHY

List of abbreviated journal titles

| | |
|---|---|
| ACS Appl Mater Interfaces | ACS applied materials & interfaces |
| Adv Drug Deliv Rev | Advanced drug delivery reviews |
| Adv Healthc Mater | Advanced healthcare materials |
| Annu Rev Biomed Eng | Annual review of biomedical engineering |
| Annu Rev Med | Annual review of medicine |
| Biomark Res | Biomarker research |
| Biomater Res | Biomaterials research |
| Biomater Sci | Biomaterials science |
| Cell Mol Immunol | Cellular & molecular immunology |
| Chem Rev | Chemical reviews |
| Chem Sci | Chemical science |
| Colloids Surf B Biointerfaces | Colloids and surfaces. B, Biointerfaces |
| Eur J Pharm Biopharm | European journal of pharmaceutics and biopharmaceutics |
| Front Cardiovasc Med | Frontiers in cardiovascular medicine |
| Int J Pharm | International journal of pharmaceutics |
| J Am Chem Soc | Journal of the American Chemical Society |
| J Biomater Sci Polym Ed | Journal of biomaterials science. Polymer edition |
| JCI insight | JCI insight |
| J Clin Invest | The Journal of clinical investigation |
| J Colloid Interface Sci | Journal of colloid and interface science |

| | |
|---|---|
| J Control Release | Journal of controlled release |
| J Interferon Cytokine Res | Journal of interferon & cytokine research |
| J Microencapsul | Journal of microencapsulation |
| J Nanobiotechnology | Journal of nanobiotechnology |
| Macromol Rapid Commun | Macromolecular rapid communications |
| Nano Lett | Nano letters |
| Nat Commun | Nature communications |
| Nat Protoc | Nature protocols |
| Nat Rev Drug Discov | Nature reviews. Drug discovery |
| Oncol Lett | Oncology letters |
| R Soc Open Sci | Royal Society open science |
| Saudi Pharm J | Saudi pharmaceutical journal |
| Sci Rep | Scientific reports |
| Sci Transl Med | Science translational medicine |
| Wiley Interdiscip Rev Nanomed Nanobiotechnol | Wiley interdisciplinary reviews. Nanomedicine and nanobiotechnology |

1 Patra, J. K. *et al.* Nano based drug delivery systems: recent developments and future prospects. *J Nanobiotechnology* **16**, 71, doi:10.1186/s12951-018-0392-8 (2018).

2 Han, X. *et al.* Ligand-tethered lipid nanoparticles for targeted RNA delivery to treat liver fibrosis. *Nat Commun* **14**, 75, doi:10.1038/s41467-022-35637-z (2023).

3 Wang, X. *et al.* Preparation of selective organ-targeting (SORT) lipid nanoparticles (LNPs) using multiple technical methods for tissue-specific mRNA delivery. *Nat Protoc* **18**, 265-291, doi:10.1038/s41596-022-00755-x (2023).

4 Khan, A. A., Alanazi, A. M., Jabeen, M., Chauhan, A. & Ansari, M. A. Therapeutic potential of functionalized siRNA nanoparticles on regression of liver cancer in experimental mice. *Sci Rep* **9**, 15825, doi:10.1038/s41598-019-52142-4 (2019).

5 Pathak, R. K., Kolishetti, N. & Dhar, S. Targeted nanoparticles in mitochondrial medicine. *Wiley Interdiscip Rev Nanomed Nanobiotechnol* **7**, 315-329, doi:10.1002/wnan.1305 (2015).

6 Li, W. Q. *et al.* Mitochondria-Targeting Polydopamine Nanoparticles To Deliver Doxorubicin for Overcoming Drug Resistance. *ACS Appl Mater Interfaces* **9**, 16793-16802, doi:10.1021/acsami.7b01540 (2017).

7 Czupiel, P., Delplace, V. & Shoichet, M. Nanoparticle delivery of a pH-sensitive prodrug of doxorubicin and a mitochondrial targeting VES-H(8)R(8) synergistically kill multi-drug resistant breast cancer cells. *Sci Rep* **10**, 8726, doi:10.1038/s41598-020-65450-x (2020).

8 Zelepukin, I. V. *et al.* Flash drug release from nanoparticles accumulated in the targeted blood vessels facilitates the tumour treatment. *Nat Commun* **13**, 6910, doi:10.1038/s41467-022-34718-3 (2022).

9 Erthal, L. C. S., Shi, Y., Sweeney, K. J., Gobbo, O. L. & Ruiz-Hernandez, E. Nanocomposite formulation for a sustained release of free drug and drug-loaded responsive nanoparticles: an approach for a local therapy of glioblastoma multiforme. *Sci Rep* **13**, 5094, doi:10.1038/s41598-023-32257-5 (2023).

10 Bai, X., Smith, Z. L., Wang, Y., Butterworth, S. & Tirella, A. Sustained Drug Release from Smart Nanoparticles in Cancer Therapy: A Comprehensive Review. *Micromachines (Basel)* **13**, doi:10.3390/mi13101623 (2022).

11 Griset, A. P. *et al.* Expansile nanoparticles: synthesis, characterization, and in vivo efficacy of an acid-responsive polymeric drug delivery system. *J Am Chem Soc* **131**, 2469-2471, doi:10.1021/ja807416t (2009).

12 Uthaman, S., Huh, K. M. & Park, I. K. Tumor microenvironment-responsive nanoparticles for cancer theragnostic applications. *Biomater Res* **22**, 22, doi:10.1186/s40824-018-0132-z (2018).

13 Mudshinge, S. R., Deore, A. B., Patil, S. & Bhalgat, C. M. Nanoparticles: Emerging carriers for drug delivery. *Saudi Pharm J* **19**, 129-141, doi:10.1016/j.jsps.2011.04.001 (2011).

14 Vrignaud, S., Benoit, J. P. & Saulnier, P. Strategies for the nanoencapsulation of hydrophilic molecules in polymer-based nanoparticles. *Biomaterials* **32**, 8593-8604, doi:10.1016/j.biomaterials.2011.07.057 (2011).

15 Zhang, H. & Grinstaff, M. W. Recent advances in glycerol polymers: chemistry and biomedical applications. *Macromol Rapid Commun* **35**, 1906-1924, doi:10.1002/marc.201400389 (2014).

16 Al Subeh, Z. Y. *et al.* Delivery of eupenifeldin via polymer-coated surgical buttresses prevents local lung cancer recurrence. *J Control Release* **331**, 260-269, doi:10.1016/j.jconrel.2021.01.026 (2021).

17 Sabatelle, R. C. *et al.* Ultra-high drug loading improves nanoparticle efficacy against peritoneal mesothelioma. *Biomaterials* **285**, 121534, doi:10.1016/j.biomaterials.2022.121534 (2022).

18 Ekladious, I. *et al.* Synthesis of poly(1,2-glycerol carbonate)-paclitaxel conjugates and their utility as a single high-dose replacement for multi-dose treatment regimens in peritoneal cancer. *Chem Sci* **8**, 8443-8450, doi:10.1039/c7sc03501b (2017).

19 Ekladious, I. *et al.* Reinforcement of polymeric nanoassemblies for ultra-high drug loadings, modulation of stiffness and release kinetics, and sustained therapeutic efficacy. *Nanoscale* **10**, 8360-8366, doi:10.1039/c8nr01978a (2018).

20 Zhang, H. & Grinstaff, M. W. Synthesis of atactic and isotactic poly(1,2-glycerol carbonate)s: degradable polymers for biomedical and pharmaceutical applications. *J Am Chem Soc* **135**, 6806-6809, doi:10.1021/ja402558m (2013).

21 Climent, E., Benaiges, D. & Pedro-Botet, J. Hydrophilic or Lipophilic Statins? *Front Cardiovasc Med* **8**, 687585, doi:10.3389/fcvm.2021.687585 (2021).

22 Glassman, P. M. *et al.* Red blood cells: The metamorphosis of a neglected carrier into the natural mothership for artificial nanocarriers. *Adv Drug Deliv Rev* **178**, 113992, doi:10.1016/j.addr.2021.113992 (2021).

23 Eloy, J. O. *et al.* Liposomes as carriers of hydrophilic small molecule drugs: strategies to enhance encapsulation and delivery. *Colloids Surf B Biointerfaces* **123**, 345-363, doi:10.1016/j.colsurfb.2014.09.029 (2014).

24 Gamboa, A. *et al.* Delivery of ionizable hydrophilic drugs based on pharmaceutical formulation of ion pairs and ionic liquids. *Eur J Pharm Biopharm* **156**, 203-218, doi:10.1016/j.ejpb.2020.09.007 (2020).

25 Iqbal, M., Zafar, N., Fessi, H. & Elaissari, A. Double emulsion solvent evaporation techniques used for drug encapsulation. *Int J Pharm* **496**, 173-190, doi:10.1016/j.ijpharm.2015.10.057 (2015).

26 Hanson, J. A. *et al.* Nanoscale double emulsions stabilized by single-component block copolypeptides. *Nature* **455**, 85-88, doi:10.1038/nature07197 (2008).

27 Schuch, A., Deiters, P., Henne, J., Kohler, K. & Schuchmann, H. P. Production of W/O/W (water-in-oil-in-water) multiple emulsions: droplet breakup and release of water. *J Colloid Interface Sci* **402**, 157-164, doi:10.1016/j.jcis.2013.03.066 (2013).

28 Chiang, C. S., Hu, S. H., Liao, B. J., Chang, Y. C. & Chen, S. Y. Enhancement of cancer therapy efficacy by trastuzumab-conjugated and pH-sensitive nanocapsules with the simultaneous encapsulation of hydrophilic and hydrophobic compounds. *Nanomedicine* **10**, 99-107, doi:10.1016/j.nano.2013.07.009 (2014).

29 Park, J. S. *et al.* The use of anti-COX2 siRNA coated onto PLGA nanoparticles loading dexamethasone in the treatment of rheumatoid arthritis. *Biomaterials* **33**, 8600-8612, doi:10.1016/j.biomaterials.2012.08.008 (2012).

30 Ordikhani, F. *et al.* Targeting antigen-presenting cells by anti-PD-1 nanoparticles augments antitumor immunity. *JCI Insight* **3**, doi:10.1172/jci.insight.122700 (2018).

31 Wang, C., Ye, Y., Hochu, G. M., Sadeghifar, H. & Gu, Z. Enhanced Cancer Immunotherapy by Microneedle Patch-Assisted Delivery of Anti-PD1 Antibody. *Nano Lett* **16**, 2334-2340, doi:10.1021/acs.nanolett.5b05030 (2016).

32 Hickey, J. W., Santos, J. L., Williford, J. M. & Mao, H. Q. Control of polymeric nanoparticle size to improve therapeutic delivery. *J Control Release* **219**, 536-547, doi:10.1016/j.jconrel.2015.10.006 (2015).

33 Hoshyar, N., Gray, S., Han, H. & Bao, G. The effect of nanoparticle size on in vivo pharmacokinetics and cellular interaction. *Nanomedicine (Lond)* **11**, 673-692, doi:10.2217/nnm.16.5 (2016).

34 Albanese, A., Tang, P. S. & Chan, W. C. The effect of nanoparticle size, shape, and surface chemistry on biological systems. *Annu Rev Biomed Eng* **14**, 1-16, doi:10.1146/annurev-bioeng-071811-150124 (2012).

35 Karal-Yilmaz, O., Serhatli, M., Baysal, K. & Baysal, B. M. Preparation and in vitro characterization of vascular endothelial growth factor (VEGF)-loaded poly(D,L-lactic-co-glycolic acid) microspheres using a double emulsion/solvent evaporation technique. *J Microencapsul* **28**, 46-54, doi:10.3109/02652048.2010.523795 (2011).

36 Pirooznia, N., Hasannia, S., Lotfi, A. S. & Ghanei, M. Encapsulation of alpha-1 antitrypsin in PLGA nanoparticles: in vitro characterization as an effective aerosol formulation in pulmonary diseases. *J Nanobiotechnology* **10**, 20, doi:10.1186/1477-3155-10-20 (2012).

37 Martinez, N. Y., Andrade, P. F., Duran, N. & Cavalitto, S. Development of double emulsion nanoparticles for the encapsulation of bovine serum albumin. *Colloids Surf B Biointerfaces* **158**, 190-196, doi:10.1016/j.colsurfb.2017.06.033 (2017).

38 Bouclier, C. *et al.* Physicochemical characteristics and preliminary in vivo biological evaluation of nanocapsules loaded with siRNA targeting estrogen receptor alpha. *Biomacromolecules* **9**, 2881-2890, doi:10.1021/bm800664c (2008).

39 Perez, C. *et al.* Poly(lactic acid)-poly(ethylene glycol) nanoparticles as new carriers for the delivery of plasmid DNA. *J Control Release* **75**, 211-224, doi:10.1016/s0168-3659(01)00397-2 (2001).

40 Kamaly, N., Yameen, B., Wu, J. & Farokhzad, O. C. Degradable Controlled-Release Polymers and Polymeric Nanoparticles: Mechanisms of Controlling Drug Release. *Chem Rev* **116**, 2602-2663, doi:10.1021/acs.chemrev.5b00346 (2016).

41 Wang, Y. *et al.* Cisplatin nanoparticles boost abscopal effect of radiation plus anti-PD1 therapy. *Biomater Sci* **9**, 3019-3027, doi:10.1039/d1bm00112d (2021).

42 Gu, G. J. *et al.* Mannosylated-serum albumin nanoparticle imaging to monitor tumor-associated macrophages under anti-PD1 treatment. *J Nanobiotechnology* **21**, 31, doi:10.1186/s12951-023-01791-9 (2023).

43 Song, Y. *et al.* Albumin nanoparticle containing a PI3Kgamma inhibitor and paclitaxel in combination with alpha-PD1 induces tumor remission of breast cancer in mice. *Sci Transl Med* **14**, eabl3649, doi:10.1126/scitranslmed.abl3649 (2022).

44 Liu, F. *et al.* Enzyme-catalyzed degradation of biodegradable polymers derived from trimethylene carbonate and glycolide by lipases from Candida antarctica and Hog pancreas. *J Biomater Sci Polym Ed* **23**, 1355-1368, doi:10.1163/092050611X581525 (2012).

45 Zhang, Z., Kuijer, R., Bulstra, S. K., Grijpma, D. W. & Feijen, J. The in vivo and in vitro degradation behavior of poly(trimethylene carbonate). *Biomaterials* **27**, 1741-1748, doi:10.1016/j.biomaterials.2005.09.017 (2006).

46 Newick, K., O'Brien, S., Moon, E. & Albelda, S. M. CAR T Cell Therapy for Solid Tumors. *Annu Rev Med* **68**, 139-152, doi:10.1146/annurev-med-062315-120245 (2017).

47 Chen, L. & Han, X. Anti-PD-1/PD-L1 therapy of human cancer: past, present, and future. *J Clin Invest* **125**, 3384-3391, doi:10.1172/JCI80011 (2015).

48 Sharma, P. & Allison, J. P. Immune checkpoint targeting in cancer therapy: toward combination strategies with curative potential. *Cell* **161**, 205-214, doi:10.1016/j.cell.2015.03.030 (2015).

49 Simon, S. & Labarriere, N. PD-1 expression on tumor-specific T cells: Friend or foe for immunotherapy? *Oncoimmunology* **7**, e1364828, doi:10.1080/2162402X.2017.1364828 (2017).

50 Upadhaya, S., Neftelinov, S. T., Hodge, J. & Campbell, J. Challenges and opportunities in the PD1/PDL1 inhibitor clinical trial landscape. *Nat Rev Drug Discov* **21**, 482-483, doi:10.1038/d41573-022-00030-4 (2022).

51 Chen, Q., Wang, C., Chen, G., Hu, Q. & Gu, Z. Delivery Strategies for Immune Checkpoint Blockade. *Adv Healthc Mater* **7**, e1800424, doi:10.1002/adhm.201800424 (2018).

52 Tran, T. H. & Phuong Tran, T. T. Targeting the PD-1/PD-L1 axis for cancer treatment: a review on nanotechnology. *R Soc Open Sci* **9**, 211991, doi:10.1098/rsos.211991 (2022).

53 Yu, X., Fang, C., Zhang, K. & Su, C. Recent Advances in Nanoparticles-Based Platforms Targeting the PD-1/PD-L1 Pathway for Cancer Treatment. *Pharmaceutics* **14**, doi:10.3390/pharmaceutics14081581 (2022).

54 Grosser, R., Cherkassky, L., Chintala, N. & Adusumilli, P. S. Combination Immunotherapy with CAR T Cells and Checkpoint Blockade for the Treatment of Solid Tumors. *Cancer Cell* **36**, 471-482, doi:10.1016/j.ccell.2019.09.006 (2019).

55 Cherkassky, L. *et al.* Human CAR T cells with cell-intrinsic PD-1 checkpoint blockade resist tumor-mediated inhibition. *J Clin Invest* **126**, 3130-3144, doi:10.1172/JCI83092 (2016).

56 Pistillo, M. P. *et al.* IFN-gamma upregulates membranous and soluble PD-L1 in mesothelioma cells: potential implications for the clinical response to PD-1/PD-L1 blockade. *Cell Mol Immunol* **17**, 410-411, doi:10.1038/s41423-019-0245-x (2020).

57 Jorgovanovic, D., Song, M., Wang, L. & Zhang, Y. Roles of IFN-gamma in tumor progression and regression: a review. *Biomark Res* **8**, 49, doi:10.1186/s40364-020-00228-x (2020).

58 Balachandran, S. & Adams, G. P. Interferon-gamma-induced necrosis: an antitumor biotherapeutic perspective. *J Interferon Cytokine Res* **33**, 171-180, doi:10.1089/jir.2012.0087 (2013).

59 Zheng, Y., Fang, Y. C. & Li, J. PD-L1 expression levels on tumor cells affect their immunosuppressive activity. *Oncol Lett* **18**, 5399-5407, doi:10.3892/ol.2019.10903 (2019).

60 Soliman, H., Khalil, F. & Antonia, S. PD-L1 expression is increased in a subset of basal type breast cancer cells. *PLoS One* **9**, e88557, doi:10.1371/journal.pone.0088557 (2014).

# CURRICULUM VITAE